NUREG/CR-1404
BNL-NUREG-51179
AN, R-7

TRANSIENT ANALYSIS OF COOLANT FLOW AND HEAT TRANSFER IN LMFBR PIPING SYSTEMS

IMTIAZ K. MADNI

Manuscript Completed - March 1980
Date Published - April 1980

ENGINEERING AND ADVANCED REACTOR SAFETY DIVISION
DEPARTMENT OF NUCLEAR ENERGY, BROOKHAVEN NATIONAL LABORATORY
UPTON, NEW YORK 11973

PREPARED FOR THE UNITED STATES NUCLEAR REGULATORY COMMISSION
OFFICE OF NUCLEAR REGULATORY RESEARCH
WASHINGTON, D.C. 20555
NRC FIN NO. A-3015

NOTICE

Available from
GPO Sales Program
Division of Technical Information and Document Control
U.S. Nuclear Regulatory Commission
Washington, D.C. 20555
and
National Technical Information Service
Springfield, Virginia 22161

ABSTRACT

A one-dimensional model for transient analysis of coolant flow and heat transfer in LMFBR piping systems is presented, in which energy equations are formulated for the coolant and pipe wall using the nodal heat balance approach. An implicit integration scheme is applied to the coolant equation with explicit wall heat flux, allowing the solution to march in the flow direction. Uncertainties in Nusselt number correlations are shown to have the greatest impact on overall heat transfer coefficients at low flow conditions. For coolant dynamics, each pipe run between components is treated as a lumped control volume. For the transient cases studied: a) The predicted response using the coolant-wall model is in excellent agreement with a more detailed model that includes insulation heat losses, while the transport delay and coolant mixing models appear to be inadequate. b) The degree of axial nodalization required for a converged solution is indeed bounded. c) Timestep control is found to be most efficiently achieved using the characteristic time approach. d) The predicted flow decay is found to be only marginally affected by the Reynolds number dependence of friction factor in the pipings and IHX.

TABLE OF CONTENTS

LIST OF FIGURES

LIST OF TABLES

FOREWORD

As a part of the Super System Code (SSC) development project for simulating thermohydraulic transients in LMFBRs, a model for the sodium-carrying pipings in the heat transport system was developed. This topical report describes the model in detail and presents results of some sample transient cases.

This work, covered under budget activity No. 60-19-20-01-1, was performed for the Office of the Assistant Director for Advanced Reactor Safety Research, Division of Reactor Safety Research, United States Nuclear Regulatory Commission.

ACKNOWLEDGMENTS

The author is grateful to M. Khatib-Rahbar for the many useful discussions he has had with him during the preparation of this report. Thanks are also due to J. G. Guppy and R. J. Cerbone for reviewing the report, and to P. Siemen for her skilful typing of the manuscript.

2. INTRODUCTION

In a loop-type Liquid Metal-cooled Fast Breeder Reactor (LMFBR) plant, reactor-generated heat is transferred to the steam generator by means of liquid sodium flowing through large diameter stainless steel piping connecting the various components in the primary and intermediate heat transport systems. The piping runs are insulated on the outside to minimize heat losses to the ambient. As an example, Fig. 1 is a plan view of the piping system for the Clinch River Breeder Reactor Plant (CRBRP). An isometric view of one of the primary piping loops[1] for the same plant is shown in Fig. 2. The loops and bends are provided to accommodate thermal expansion imposed on the piping during operation, without exceeding acceptable stress limits. It can be seen that the piping runs are extensive, and by far the longest time the coolant will spend in its passage through the heat transport circuit is in these piping runs. Hence, a thermal-hydraulic model for coolant flow in piping should form an important part of the overall system simulation model. In pool-type designs, the pipes in the primary system, being enclosed in the main tank, are shorter and, being submerged in pool sodium, are not insulated on the outside. However, since the intermediate system is generically identical to that in loop-type designs, the pipe model would be just as important.

Due to their length, the piping runs create a significant time delay in the impact of a temperature transient as coolant is transported from the reactor to the components in the rest of the primary system, or from the steam generator to the rest of the intermediate system. This phenomenon can be represented by a simple transport time-delay model[2]. However, this is not believed to be sufficient for two reasons. Firstly, the temperature

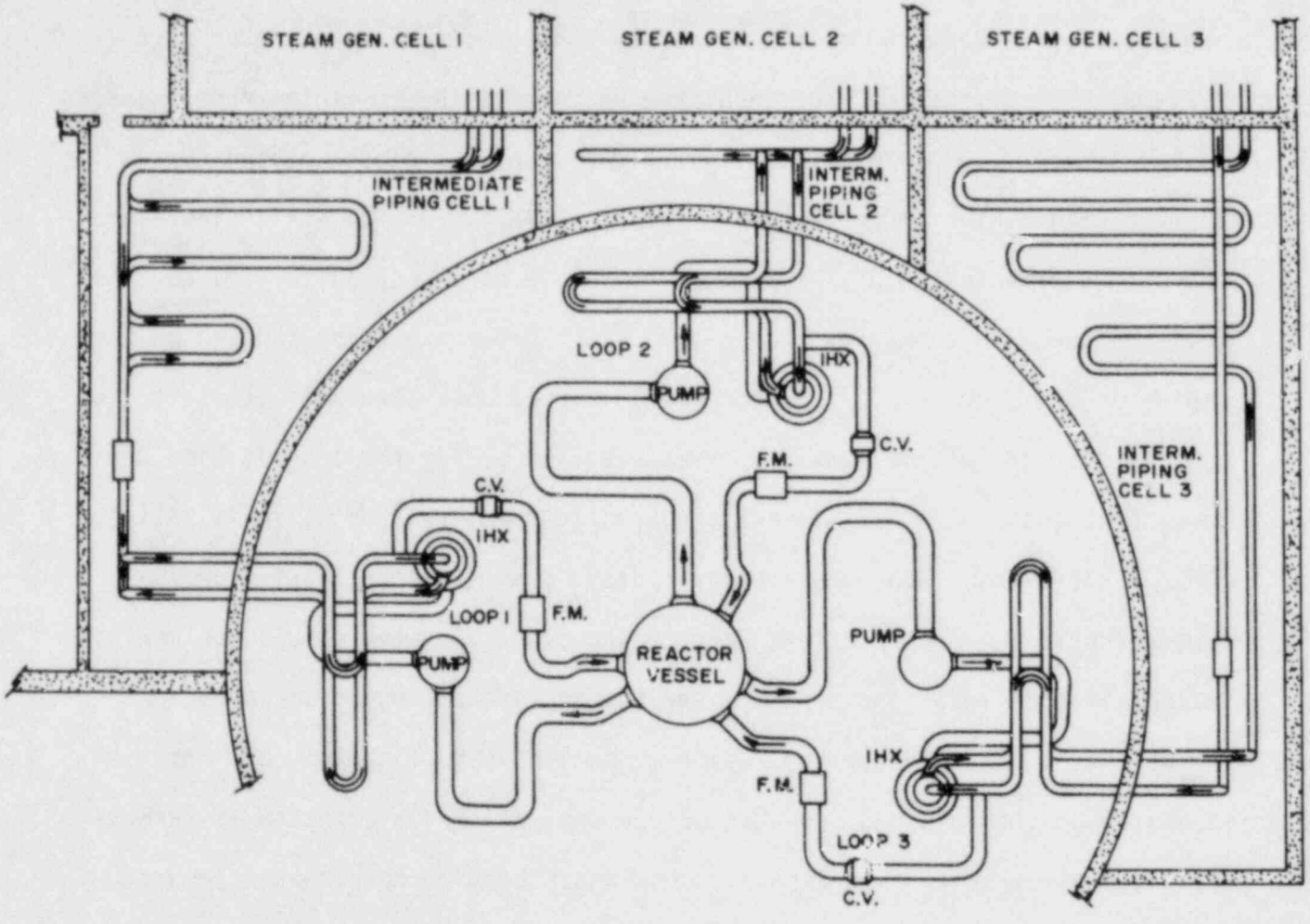

Figure 1. Plan view of CRBR Heat Transport System Piping Arrangement

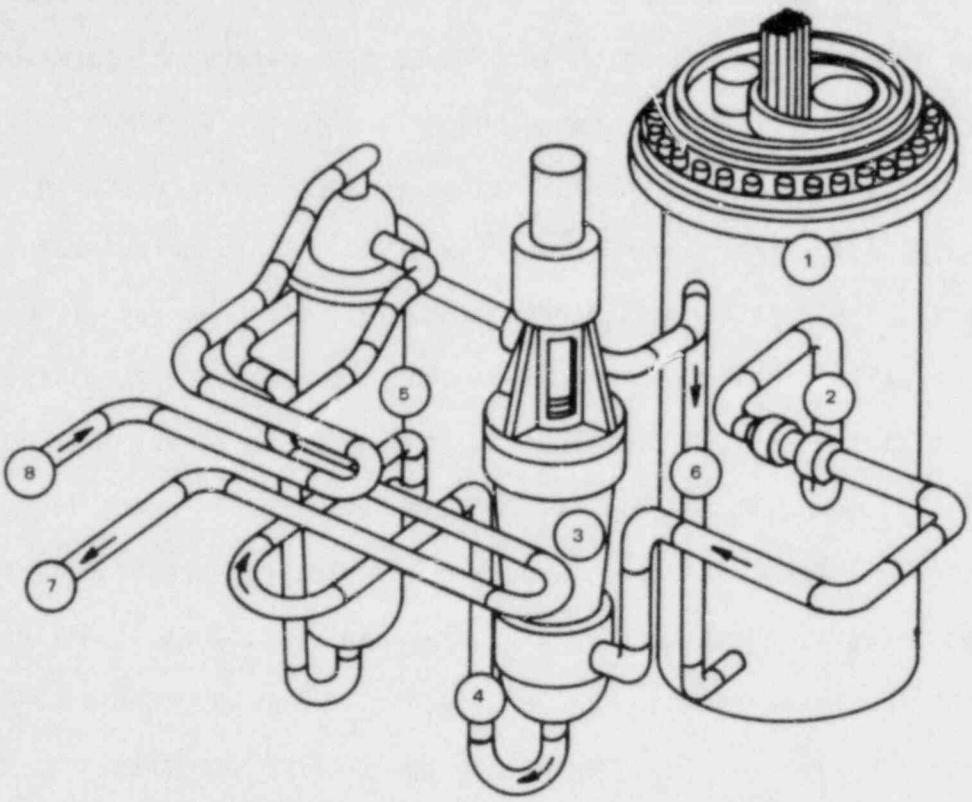

1. Reactor Vessel
2. Sodium from Reactor to Primary Pump (Hot Leg)
3. Primary Pump
4. Sodium from Primary Pump to Intermediate Heat Exchanger (Hot Leg)
5. Intermediate Heat Exchanger
6. Sodium from Intermediate Heat Exchanger to Reactor (Cold Leg)
7. Sodium from Intermediate Heat Exchanger to Superheater
8. Sodium from Intermediate Sodium Pump to Heat Exchanger

Figure 2. Isometric view of primary and portions of intermediate piping in one HTS loop of the CRBRP.

signal is not only delayed in its passage from inlet to outlet of a pipe run, but also altered. This makes it necessary to model the mixing in the fluid and heat transfer process between the coolant and pipe wall during transients. Secondly, a detailed temperature distribution is needed for a more accurate determination of the gravitational heads, hence, the natural circulation capability of the heat transport system under loss-of-forced-flow conditions.

This report describes the thermal-hydraulic model for the piping, as it has been developed for the Super System Code (SSC)[3]. The thermal model is a one-dimensional, discrete parameter representation, with two radial nodes (coolant, pipe wall) and a user specified number of axial nodes, giving rise to a spatial temperature distribution in the piping at any time during a transient. The momentum equation itself can be solved for very large control volumes since the intermediate pressures along a pipe run are of no interest (unless a leak occurs, in which case the large control volume is divided into two volumes at the break location). This is due to the incompressible nature of the flow in the piping. Thus, each pipe run between components is treated as a lumped control volume, and hydraulic equations are written in terms of pressure losses in that run. Frictional losses are accounted for by a flow-dependent friction factor. Gravity terms are dependent on system hydraulic profile (elevations) and sodium density distribution. The density of sodium at any location is a function of temperature and is evaluated from thermal calculations. Model equations for the piping, when incorporated into the system equations, will yield the temperatures, pressures and flow rates in the heat transport system.

Results of some sample transients are presented. Comparisons between the coolant-wall model and a more detailed model that includes heat loss through insulation are made to demonstrate the adequacy of the former for system simu-

lation. Also included in the comparison are the transport delay model and a coolant-mixing (adiabatic wall) model. Studies are carried out to test the sensitivity of the predicted results to degree of axial nodalization. Established correlations for Nusselt number are compared, and the impact of their uncertainties on overall heat transfer coefficient is shown. The effects of including a flow-dependent friction factor on predicted system hydraulic response as compared to a constant loss coefficient, are studied for a pump coastdown to natural circulation transient.

In the discussion on areas of future work, a brief reference is made to stratification effects and their impact on the temperature distribution within the pipe and on the validity of 1-D models for system simulation.

3. ANALYSIS

3.1 Basic Assumptions

The following assumptions are inherent in the analysis:

(1) The flow is one-dimensional, implying uniform velocity and temperature profiles normal to the flow direction for all flow regimes.

(2) The coolant is single-phase liquid. This assumption rests on the consideration that, for the events within the scope of the SSC code, sodium in the piping remains subcooled. Under normal operating conditions, the maximum temperature of sodium in the piping circuit is approximately 340K less than its saturation temperature at atmospheric pressure. Therefore, during abnormal or accident conditions, aside from the fact that temperature transients in the core are damped by the time the coolant exits from the reactor vessel, there is also a wide margin to boiling in the piping circuit.

(3) The coolant is incompressible, i.e., coolant properties are not pressure dependent. This is a good assumption for most liquids.

(4) Single mass flow rate model, i.e., at any instant of time, the mass flow rate would be uniform everywhere in a circuit, except at a free surface, or a pipe break, or branch or junction. This comes about by neglecting the time derivative of density in the continuity equation.

(5) Axial conduction in walls is neglected.

(6) Pipe walls are perfectly insulated on the outside. From a full-power heat balance for the CRBR Nuclear Steam Supply System,[4] the fraction of [redacted]or power lost to the ambient through all primary and intermediate pipe runs is 0.00055. This is small enough to justify the above assumption. The adequacy of this assumption for transients of

interest to SSC will be investigated in Chapter 4.

(7) Frictional heating is neglected.

(8) Fully developed flow and heat transfer are assumed.

3.2 Heat Transfer Model

3.2.1 Background

Analytical solutions to the energy equations in partial differential form are only available for restricted specific cases, and so a general, detailed thermal model would involve dividing the pipe section into many nodes, and then solving the energy equations locally. Several different multi-node representations are available and have been used in reactor system simulation work. Most of the investigations have been for the intermediate heat exchanger, and can be advantageously used for the piping. In 1966, Gerhardstein[5] started with the partial differential equations and finite-differenced the space-derivative terms to obtain a multi-node model consisting of a set of ordinary differential equations. He used central and backward differencing but preferred the backward difference for the Fast Flux Test Facility (FFTF) system simulation. Earlier, in 1965, Clist and Hopkinson[6] had used central differencing in their model. In 1969, Jennings[7] compared several multi-node models including the finite-difference method (backward and central difference), and the nodal heat balance method (applying energy balance over a nodal control volume) for a constant flow heat-exchanger, and concluded that nodal heat balance models were better. In 1970, Gunby[8] carried out a more general study in which he compared models under variable temperature and flow transients. A mixed-difference (alternating forward and three-point backward difference) model was also added to the comparisons. He concluded from his study that backward and central differences were the poorest performers in terms of accuracy and response. The mixed difference was considered the best, with the nodal heat

balance a close second, and hence, a good alternative.

The present analysis uses the nodal heat balance method, partly because it is simpler to formulate, and partly because it bears a physical relation to the heat transport process, making it a good model for most transients.

3.2.2 Model Features

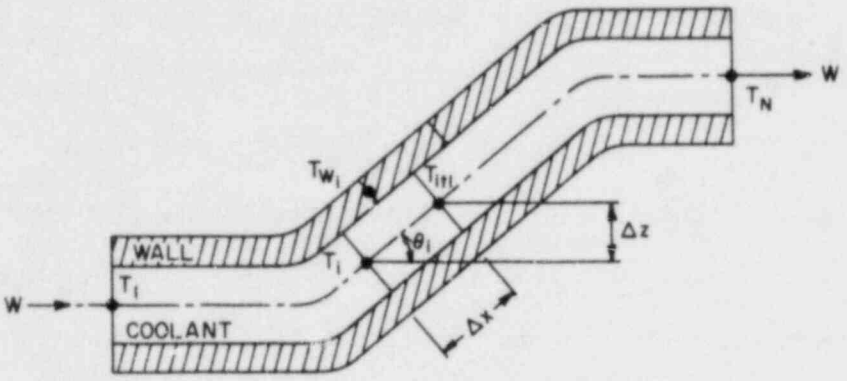

Figure 3. Model Configuration for Flow in Piping

Fig. 3 shows the model configuration. Some features of the heat transfer model are:

(1) Each pipe section is divided axially into several nodes, N, all with fixed positions in space and equidistant. Selection of the number of nodes for each pipe run is influenced by the pipe length and the coolant velocity at full flow.

(2) There are two radial nodes (coolant and pipe wall), forming a staggered arrangement, as shown in the figure. Heat transfer between coolant and and pipe wall is included.

(3) The energy equation is applied locally, using nodal heat balance.

(4) Heat transfer coefficients are evaluated locally as functions of temperature and flow conditions.

(5) Material properties are expressed as curve-fitted polynomial functions of temperature.

Other features, not mentioned here, will become apparent in the subsequent discussions.

3.2.3 Governing Equations

Energy balance is applied over the control volume formed between two adjacent fluid nodes to give the coolant equation, and the wall equation is related to the coolant equation through the heat flux term. The equations can be written for i = 1 to N - 1 as follows:

Coolant:

$$\rho_{i,\,i+1}\ V \frac{de_{i+1}}{dt} = W\,(e_i - e_{i+1}) - U_{cw}A_{cw}\left[T_{i,\,i+1} - T_{w_i}\right] \qquad (1)$$

where e_{i+1} is the coolant enthalpy at node i+1, $T_{i,\,i+1}$ is the average coolant temperature in the control volume between nodes i and i+1, expressed as:

$$T_{i,\,i+1} = \frac{T_i + T_{i+1}}{2} \qquad (2)$$

$\rho_{i,\,i+1}$ is the coolant density corresponding to $T_{i,\,i+1}$, W is the mass flow rate in the pipe, V is the coolant volume between nodes i and i + 1, U_{cw} is the overall heat transfer coefficient between coolant and wall, evaluated at the midpoint between coolant nodes i and i + 1, and A_{cw} is the area for heat

transfer between coolant and wall, given by

$$A_{cw} = \pi D_i \Delta x \tag{3}$$

Inherent in Eq. (1) is the assumption that

$$\frac{de_{i+1}}{dt} \approx \frac{de_{i,\,i+1}}{dt} \tag{4}$$

This approximation, commonly referred to as 'donor cell' approach, has some advantages in minimizing numerical diffusion effects.[8]

Wall:

$$M_w C_{w_i} \frac{dT_{w_i}}{dt} = U_{cw} A_{cw} \left[T_{i,\,i+1} - T_{w_i} \right] \tag{5}$$

where M_w is the mass of wall of length Δx, and C_{w_i} its temperature-dependent specific heat.

3.2.4 Finite-difference Forms

A fully implicit single-layer time integration scheme is applied to Eq. (1), with the exception of the wall heat flux term, which is allowed to be determined explicitly. With this, Eq. (1) becomes:

$$\rho^k_{i,\,i+1} V \frac{\left(e^{k+1}_{i+1} - e^k_{i+1} \right)}{h} = W^{k+1} \left(e^{k+1}_i - e^{k+1}_{i+1} \right) - U^k_{cw} A_{cw} \left(T^k_{i,\,i+1} - T^k_{w_i} \right) \tag{6}$$

and Eq. (5) becomes

$$M_w C^k_{w_i} \frac{\left(T^{k+1}_{w_i} - T^k_{w_i} \right)}{h} = U^k_{cw} A_{cw} \left(T^k_{i,\,i+1} - T^k_{w_i} \right) \tag{7}$$

where the index k represents previous time, k+1 represents the current (advanced) time, and h is the size of the timestep. W^{k+1} is the current value of coolant flow rate. When computing the pipe module on a stand-alone basis (i.e., decoupled from system), W and inlet temperature signal T_1 would have to be input as a function of time. Equations (6) and (7) are uncoupled, and unknowns e_{i+1}^{k+1} and $T_{w_i}^{k+1}$ can be determined algebraically in a marching fashion going from i=1 to N-1. In a system model, the inlet temperature signal to the pipe run is obtained as boundary condition from its preceeding component, and W is obtained from system hydraulic calculations.

Note that Equations (6) and (7) are for forward flow only. However, the model as implemented in the code is formulated in terms of general node counters, so that the equations, the marching direction and inlet boundary conditions for each pipe section are automatically adjusted depending on the flow direction, be it forward or reverse.

Equation (7) is explicit. However, due to its large time constant, the stability limit on timestep is much larger than the maximum step sizes to be used by the code based on numerical accuracy considerations.

For accuracy, h is decided based on the relative change in the variables during the timestep, as follows:

$$h^{new} = 2h^{old} \quad \text{if } o < \varepsilon < \varepsilon_1 \qquad (8)$$

$$= h^{old} \quad \text{if } \varepsilon_1 < \varepsilon < \varepsilon_2$$

Here, $\varepsilon = \left|x^{k+1} - x^k\right| / x^o$, and ε_1 ε_2 provide the user-specified convergence band. In this study, the recommended value for $\varepsilon_1 = 0.001$, with $\varepsilon_2 = 2\varepsilon_1$. The variable x is tested for temperatures at all nodes, and the largest change is then selected for ε. If ε is greater than ε_2, the calculation is repeated with $h^{new} = 0.5h^{old}$.

The size of timestep is also limited by the transit time for coolant or the temperatur signal to travel from one node to the next, i.e.

$$h \leq \frac{\rho V}{|W|} \tag{9}$$

Since the convective term in Eq. (6) is implicit, this is not a stability limitation. This limitation is more restrictive for smaller Δx, or larger number of nodes. Also, allowable h becomes larger with decreasing flow.

To derive the stability limitation for Eq. (6), we can use the 'common sense' method due to Karplus[9], which gives

$$h \leq \frac{2\rho V C_p}{U_{cw} A_{cw}} \tag{10}$$

This constraint arises due to the explicit formulation of the heat flux term. Both Eqs. (9) and (10) have to be satisfied simultaneously.

Alternately, the characteristic time for T_{i+1} in Eq. (1) can be evaluated[10] (see appendix A) as

$$\tau_c = \rho V C_p \Big/ \left(W C_p + 0.5\, U_{cw} A_{cw} \right) \tag{11}$$

If $h \leq \tau_c$ is used, Eq. (11) reduces to Eq. (9) for an adiabatic wall and to Eq. (10) for zero flow. Thus, $h \leq \tau_c$, where τ_c is given by Eq. (11), gives the combined stepsize limitation. An example of the growth of timestep based on Eqs. (8) and (11) will be given in the next chapter.

3.2.5 Heat Transfer Coefficients

In Eqs. ( ) and (5), U_{cw} is the overall heat transfer coefficient between coolant and pipe wall, and is defined, based on the resistance concept, as

$$\frac{1}{U_{cw}} = \frac{1}{h_{film}} + r_{wall} \tag{12}$$

where r_{wall} is defined in Eq. (16), and the film heat transfer coefficient is given in terms of Nusselt numer Nu_c as

$$h_{film} = \frac{Nu_c \, k_c}{D_i} \tag{13}$$

k_c is the thermal conductivity of the coolant, and D_i is the pipe inner diameter.

Correlations for convective (film) heat transfer coefficients in pipes are generally based on either a uniform temperature of a uniform heat flux at the wall; for fully developed profiles, the coefficient with uniform heat flux being higher than that with uniform wall temperature. For flow in LMFBR sodium piping, the type of wall boundary condition applicable will depend on the response of wall temperature to changes in coolant temperature distribution. In general, if the wall temperature follows the coolant temperature changes, the more appropriate boundary condition is uniform heat flux. This will depend on the ratio of wall to coolant heat capacities. Typical values of these ratios for CRBRP and FFTF primary piping are provided in Table I. In all cases, since the wall heat capacity is lower than the coolant heat capacity, the wall temperature will closely follow the temperature distribution in the coolant, and hence, uniform heat flux is the appropriate boundary condition.

TABLE I

Heat capacity ratio of pipe wall to coolant

Plant	$(MC)_w/(MC)_c$	
	Hot leg	Cold leg
CRBRP	0.250	0.355
FFTF	0.235	0.392

Nusselt number is correlated in the SSC code in the general form as

$$Nu_c = A + B\,(\overline{\psi}\,Pe)^C \qquad (14)$$

For the calculations thus far, the coefficients A, B, C and $\overline{\psi}$ have been provided by Aoki's correlation for fully developed turbulent flow of liquid metal in a pipe, under uniform heat flux[11]:

$$Nu_c = 6.0 + 0.025\,(\overline{\psi}\,Pe)^{0.8} \qquad (15)$$

where

$$\overline{\psi} = \frac{0.014\,(1 - e^{-71.8X})}{X},$$

$$X = -\frac{1}{Re^{0.45}\,Pr^{0.2}}.$$

Fig. 4 shows comparisons among some commonly used correlations for uniform heat flux, with Pr = 0.0044, in the Peclet number range from 20 to 100,000. As an example of the range to be expected, for the CRBRP primary piping, under full flow, Reynolds number (Re)$\simeq 10^7$ and Pe $\simeq$ 45,000; at 2% flow, Re$\simeq 2 \times 10^5$ and Pe $\simeq$ 900. It is unlikely for Pe to go below 100 in the piping, except during a pipe break accident, when flows can reverse. Within the IHX tube bundle, however, Pe is much lower, ranging from 700 during full flow to about 14 at 2% flow.

All the correlations shown in Fig. 4 agree with certain sets of experimental data[12]. The Aoki correlation compares very well with the measurements of Kuroyanagi, et al.[13] for fully developed flow of liquid sodium in a nickel tube, under uniform heat flux, in the Pe range from 100 to 500. However, the correlations exhibit some deviations among themselves. The maximum deviation occurs at low Peclet numbers (Pe$\simeq$100), where the difference between the Lyon-Martinelli

and Subbotin correlations is greater than 25%. The Aoki correlation lies between the two. They all converge at higher values of Pe, where the deviations are minimal.

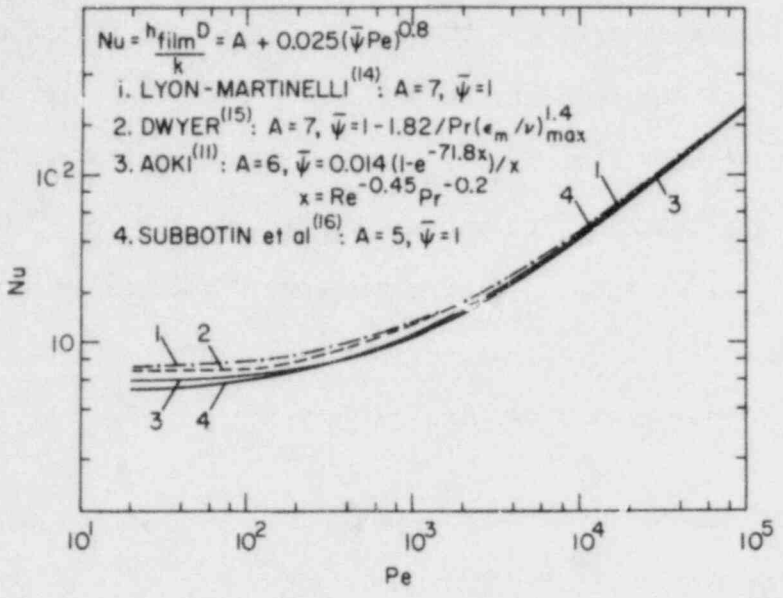

Figure 4. Comparison of Nusselt numbers from correlations for liquid metals (Pr = 0.0044) with uniform wall heat flux.

In Eq. (10), the wall resistance term is obtained by considering half the wall thickness (since that is where T_{w_i} is defined), and is expressed as

$$r_{wall} = \frac{D_i}{2} \frac{\ell n\left(\frac{D_i + D_o}{2D_i}\right)}{k_w}, \qquad (16)$$

where D_i, D_o are the pipe inner and outer diameters, respectively, and k_w is the thermal conductivity of wall material.

In Fig. 5, the behavior of $\frac{1}{h_{film}}$, r_{wall} and $\frac{1}{U_{cw}}$ for the CRBR primary piping (vessel-to-pump), is plotted over Reynolds numbers ranging from 4×10^4 to 2×10^7. The wall resistance is assumed constant. For low Re, the film resistance is predominant, whereas at high Re, the film resistance becomes very small, and nearly all the resistance is due to the wall. Fig. 6 shows the behavior of the conductance U_{cw}, h_{film} and $\frac{1}{r_{wall}}$ over the same Re range. It can be seen that U_{cw} is always limited by the smaller component of conductance. Thus, at low Re, where h_{film} is smaller, U_{cw} is limited by h_{film}, and, at higher Re as h_{film} increases very dramatically, and to a much higher value than $\frac{1}{r_{wall}}$, U_{cw} approaches the wall conductance. Any further increases in h_{film} have only a marginal effect on U_{cw}.

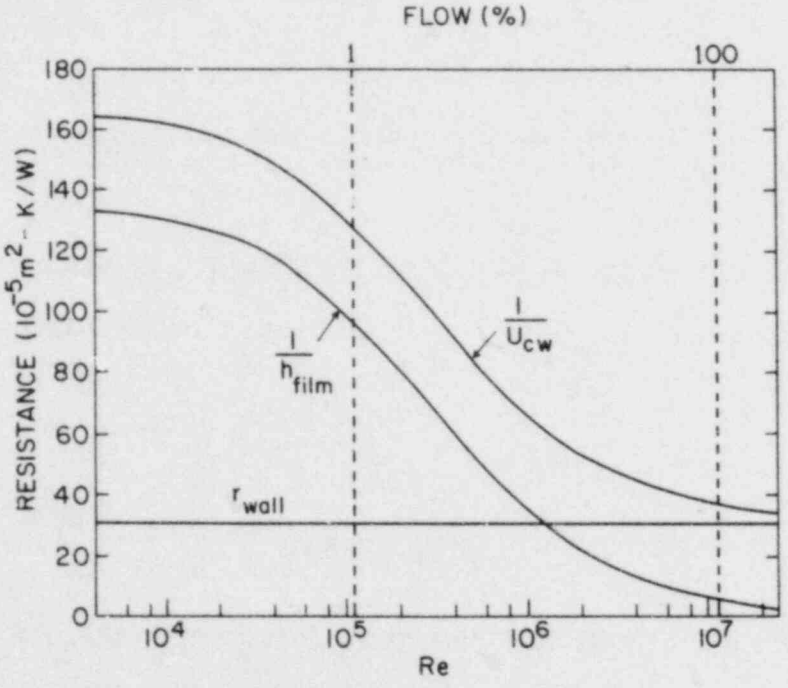

Figure 5. Thermal resistances as a function of Reynolds number for the CRBR primary piping (vessel-to-pump).

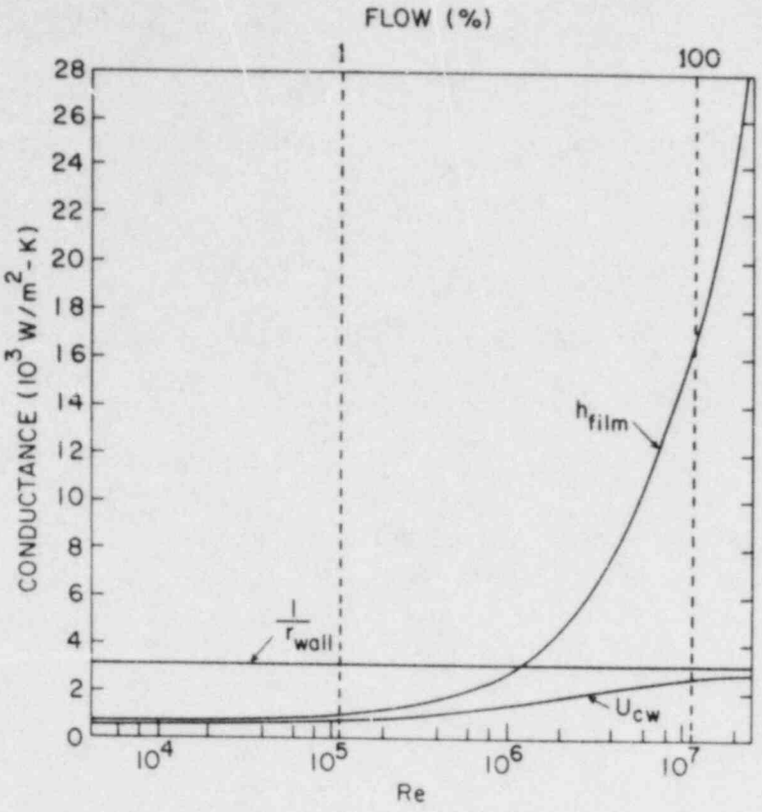

Figure 6. Thermal conductances as a function of Reynolds number for the CRBR primary piping (vessel-to-pump).

Assuming a 10% uncertainty in the evaluation of h_{film} via the Aoki correlation, we can examine its effect on the calculation of U_{cw}. Eq. (12) can be re-written as

$$U_{cw} = \frac{h_{film}}{r_{wall}\, h_{film} + 1} \tag{17}$$

Expressed in perturbation form, this becomes

$$\Delta U_{cw} = \frac{\Delta h_{film}}{(r_{wall}\, h_{film} + 1)^2} \tag{18}$$

In Eq. (18), if Δh_{film} is the uncertainty in h_{film}, ΔU_{cw} give the uncertainty in U_{cw}.

At Pe = 40,000 (full flow), h_{film} = 14,728 W/m^2 - K, and, with a Δh_{film} = 0.1 and r_{wall} = 0.00031, Eq. (18) gives ΔU_{cw} = 0.003, or 0.3%. At Pe = 1000 (2% flow), h_{film} = 1312 W/m^2 - K, and ΔU_{cw} = 0.05 or 5%. Thus, for a given uncertainty in h_{film}, the uncertainty in U_{cw} is greater at lower values of h_{film}.

In the laminar region (Re $\leq$ 3000 or Pe $\leq$ 13.2), the Nusselt number is derived theoretically[17] for uniform heat flux, as

$$Nu = 4.364 \tag{19}$$

This value is independent of the coolant flowing through the pipe.

3.3 Fluid Flow Model

3.3.1 Pressure Losses

The pressure losses in the pipe section are calculated as

$(\Delta P_{f,g})_{pipe}$ = acceleration loss + frictional loss + gravity loss (gain) + other losses.

$$= \frac{W^2}{A^2}\left(\frac{1}{\rho_N} - \frac{1}{\rho_1}\right) + \frac{1}{2}\frac{W|W|}{D_e A^2}\int_0^L \frac{f}{\rho}\,dx + g\int_0^L \rho\sin\theta\,dx$$

$$+ K\frac{W|W|}{\bar{\rho}A^2} \tag{20}$$

where f is a flow-dependent friction factor (see next subsection for details), and ρ is the coolant density. Since $\frac{f}{\rho}$ is a continuous function, $\int_0^L \frac{f}{\rho}\,dx$ can be evaluated using Simpson's rule. θ_i (see Fig. 3) is the effective flow angle

between nodes i and i+1 of the pipe run, and $\sin\theta_i$ is evaluated as $\frac{\Delta z}{\Delta x}$ where Δz is the elevation change and Δx the axial distance along the pipe from i to i+1. Since $\sin\theta_i$ depends on the pipe geometry and is, in general, not a continuous function, Simpons' rule is not applicable and the integral $\int_0^L \rho \sin\theta \, dx$ is evaluated through the summation $\Delta x \sum_{i=1}^{N-1} \rho_{i,i+1} \sin\theta_i$. K in Eq. (20) is a loss coefficient to account for losses due to bends, fittings, etc.

The importance of these pressure loss evaluations will be seen in the discussion of Section 3.5.

3.3.2 Friction Factor

The friction factor, f, depends on the Reynolds number (Re) of the flow, and the surface roughness (ε) of the pipe or channel. Curves of f vs. Re for various values of surface roughness are provided in the Moody chart. For commercial steel, $\varepsilon = 0.000046$ m.[17] It is most likely that the reactor pipes will be even smoother that this. The curves for turbulent flow in the Moody chart are generated by the Colebrook relation[19]:

$$\frac{1}{\sqrt{f}} = -2.0 \log_{10}\left(\frac{\varepsilon/D_e}{3.7} + \frac{2.51}{Re\sqrt{f}}\right) \tag{21}$$

where D_e is the hydraulic or equivalent diameter in the case on non-circular channels. Note that f is the Weisbach friction factor. Another form of the friction factor, called the Fanning friction factor (f_F), is related to f by

$$f = 4f_F \tag{22}$$

For smooth pipes, i.e., for $\varepsilon/D_e = 0$, Eq. (21) simplifies to the following transcendental equation:

$$\frac{1}{\sqrt{f}} = 2.0 \log_{10} (Re\sqrt{f}) - 0.80 \tag{23}$$

which is the same as Prandtl's Universal Law of friction for smooth pipes.[20]

A simplified form of friction factor rather than the above-mentioned transcendental equation is desirable, and the following explicit relation for f,[21] which is accurate to within ±5%, was examined:

$$f = 0.0055 \left\{ 1 + \left[20{,}000 \frac{\varepsilon}{D_e} + \frac{10^6}{Re} \right]^{1/3} \right\} \tag{24}$$

For smooth pipes, the above equation reduces to

$$f = 0.0055 + 0.55(Re)^{-1/3}, \tag{25}$$

which is very similar in form to the Koo correlation[22].

A comparison for computing efficiency in calculating f from either Eq. (21) or Eq. (24) was made. The approximate representation, Eq. (24), was found to be 25% more efficient. Since the friction factor needs to be evaluated for each node section of each pipe run, this can result in substantial savings in computing time every timestep.

The friction factor for laminar flow, i.e., $Re \leq 2000$, is given by[21]

$$f = \frac{64}{Re} \tag{26}$$

A linear interpolation for f is used in the transition region, i.e., $2000 \leq Re \leq 3000$.

Note that the Moody charts are for isothermal fluid flow. In the presence of heat transfer at the wall, either the fluid properties, such as μ, ρ should be evaluated at a 'film' temperature = $(T_w + T_b)/2$, where T_w is the wall temperature and T_b the bulk temperature of coolant, or the computed value for f should be modified by the Seider and Tate relation[21]

$$f_{modified} = f\left(\frac{\mu_w}{\mu_b}\right)^{0.14} \tag{27}$$

For flow in pipes, under steady-state, $f_{modified} = f$. Under transient, $f_{modified} \neq f$. However, this difference is considered small enough to be neglected. In fact, it is not uncommon in system codes to lump frictional and form loss into an overall $CW|W|$, where C remains unchanged during transients. A sample transient will be presented in the next chapter to compare predicted flow decay using variable frictional factors and the constant loss coefficient.

3.4 Steady-State Model

To compute the steady-state conditions (pre-transient initialization), the energy equations are solved by setting the time derivatives to zero. With the assumption of perfect insulation, the wall equation reduces to

$$T_{w_i} = \frac{T_i + T_{i+1}}{2} \quad \text{for } i = 1 \text{ to } N - 1 \tag{28}$$

and the coolant equation to

$$T_i = T_1 \quad \text{for } i = 1 \text{ to } N. \tag{29}$$

This equation also implies constant fluid properties over the pipe run.

The formulation for pressure losses in the piping is the same as for transient, except that the acceleration term drops out, and f and ρ are constant, simplifying the evaluation of the frictional loss term. Since under steady-state, momentum balance yields

$$\text{pressure drop} = \text{pressure losses}, \tag{30}$$

there being no flow transient, the terms 'loss' and 'drop' can be used interchangeably. Generally, the term 'drop' is used in the steady-state analysis.

3.5 System Thermal-hydraulics

Fig. 7 is an example configuration of the primary heat transport system of a loop-type LMFBR plant, for two-loop simulation of a multi-loop system. One of the loops has a pipe-break near the reactor vessel and all intact loops are lumped together as the other loop. The physical arrangement corresponds to the CRBR (or FFTF) design. For a pump coastdown transient, one loop simulation with all loops being lumped together is sufficient. The configuration would look much like Fig. 7 without the broken loop. In our discussions here, we focus attention on the primary system due to its more direct impact on core flow. Similar analysis is performed for the intermediate circuits.

Transient flow rates are described by volume-averaged momentum equations of the form

$$\frac{dW}{dt}\sum\frac{L}{A} = P_{in} - P_{out} - \sum\Delta P_{f,g} \tag{31}$$

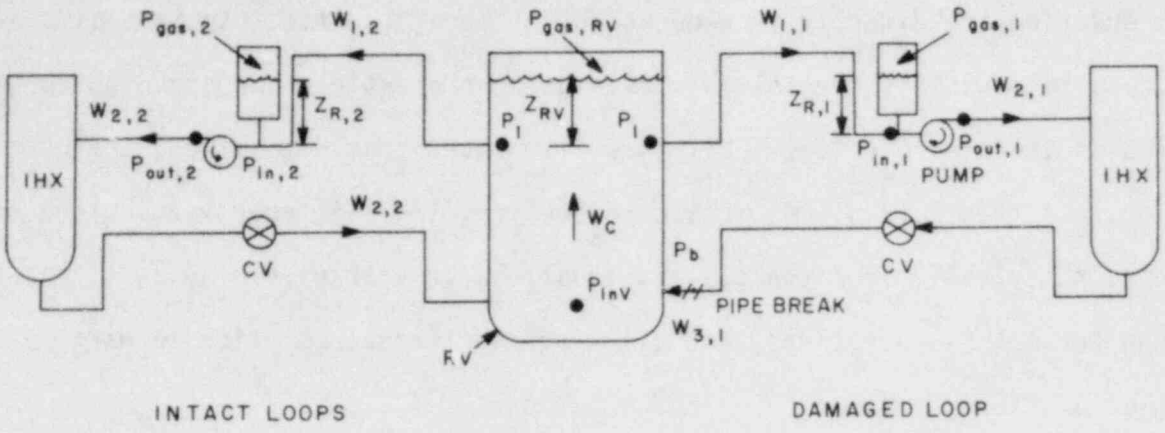

Figure 7. Primary system configuration for two-loop simulation

for each uniform mass flow rate section. Here, $\sum \frac{L}{A}$ is the fluid inertia; P_{in}, P_{out} are the endpoint pressures; and $\sum \Delta P_{f,g}$ is the sum of frictional loss, gravitational head, and other losses in the pipes and/or components in the section. For each pipe, the losses have been defined by Eq. (20).

Equation (31) for each section, together with equations for pumps, levels, vessel inlet pressure, and, in case of pipe rupture, equations for break, guard vessel, etc. form a system of ordinary differential equations and associated algebraic equations to be solved together to yield the flow rates, pressure and free surface levels in the system. These equations are solved using a sophisticated predictor-corrector algorithm of the Adams type.

Sodium properties in the heat transport system are assumed to be functions of temperature only. In addition, they are seen to be very weak functions of temperature. This enables us to almost decouple the momentum equation from the energy equation, the only coupling being through temperature dependent material properties, and allows them to be solved separately. However, the energy equation is strongly coupled to the momentum equation, since convective terms in the

energy equation are directly flow-dependent. Therefore, for transient simulation, the hydraulic equations are solved first, using properties corresponding to temperatures at the previous time. With new flow rates thus determined, the energy equations are then solved. As mentioned earlier, the wall energy equations are decoupled numerically from the coolant equations in each pipe module, eliminating the need for matrix inversions, and allowing the thermal solution to march in the direction of flow.

4. RESULTS

4.1 Stand-alone Testing

A sample transient representing a fairly severe temperature downramp of 127K in 80 seconds (which may occur at a heat exchanger outlet), was applied to a pipe section (see Fig. 8) with flow decaying according to

$$W = W_{ref} \left(1 - \frac{t}{t + \delta}\right) \text{ kg/s.} \tag{32}$$

For the stand-alone test case, Eq. (32) is a good approximation[23] to the flow coastdown that would be obtained from solution of the coolant dynamic equations. Values of $W = 805.1$ kg/s and $\delta = 5.5$ s were used.

4.1.1 Model Selection

Fig. 8 compares the predicted outlet temperature response from the coolant-wall model with a more detailed formulation that includes heat losses through insulation (see Appendix B). Also included in the comparison are the transport delay model (see Appendix C for calculations) and a coolant mixing (adiabatic wall) model. Excellent agreement is observed between the coolant-wall model and the more detailed reference model, the maximum deviation being less than 0.1K. The insulation conductivity used was 0.065 W/m-K. When this was doubled to 0.13 W/m-K, the maximum deviation was still less than 0.2K. In contrast, the transport delay and coolant mixing models are seen to grossly underpredict the outlet temperature. Earlier, Johnson[24] had compared predictions from the detailed model with the transport delay predictions and with a 2-radial node model, but using coolant and insulation (instead of the wall) nodes, and concluded that the 2-radial node model was inadequate. In his comparisons, if he had used the coolant-wall model (also a 2 radial-node model), his conclusion would have been different.

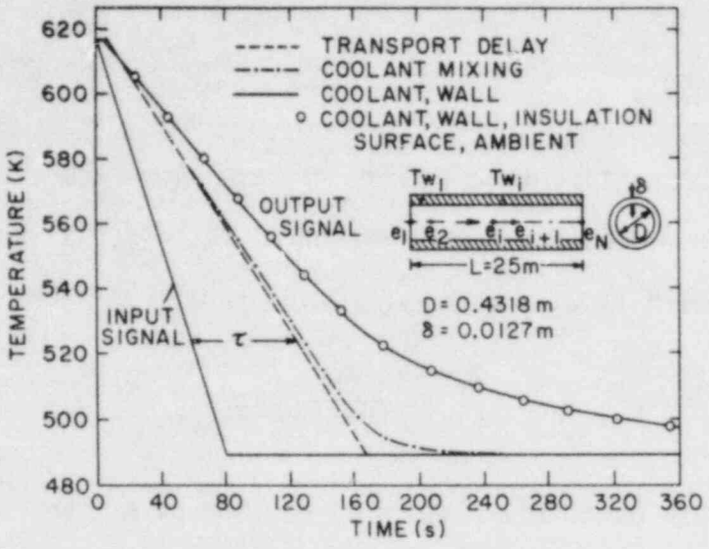

Figure 8. Comparison of predicted coolant temperatures at pipe outlet using various models

4.1.2 Nodalization

Fig. 9 examines the sensitivity of the predicted outlet signal to axial nodalization. The maximum deviation between N = 3 and N = 5 is 4K, decreasing to less than 0.5K between N = 20 and 40, and converging for $N \geq 40$. A good number to use for system simulation would be $N \geq 2(\theta + 1)$, where θ is the coolant transport time in seconds at full flow. For the sample transient considered, this corresponds to $N \geq 10$.

4.1.3 Accuracy and Growth of Timestep

In Fig. 10 we see that the computed outlet temperature response is insensitive to the selection of ε_1, ε_2 in the accuracy criterion of Eq. (8). This can be explained by examining Fig. 11, where the growth of timestep with transient time is shown plotted along with the growth of the characteristic time, τ_c, Eq. (11). With $\varepsilon_1 = 0.001$, the timestep size is controlled by Eq. (8) for the first 265 seconds, after which it follows the growth of τ_c. With $\varepsilon_1 = 0.01$, the growth

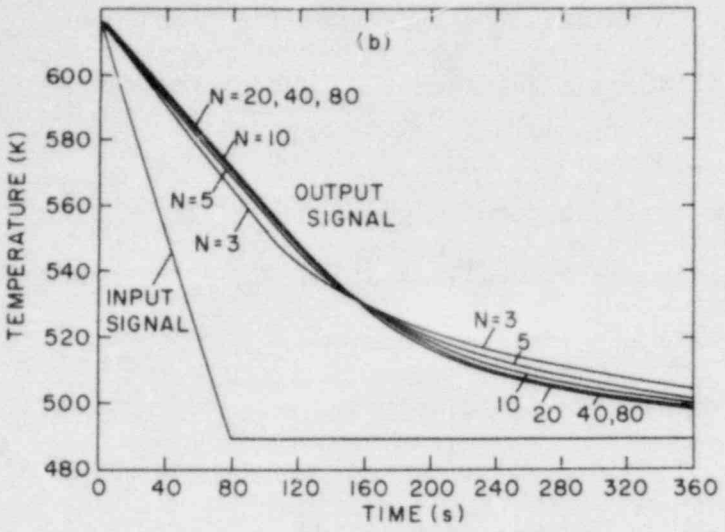

Figure 9. Sensitivity of predicted outlet temperature response to axial nodalization.

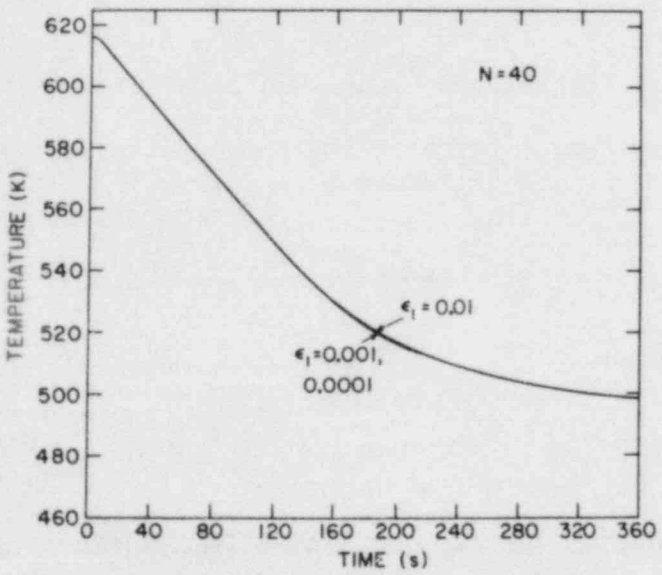

Figure 10. Sensitivity of predicted outlet temperature response to the selection of ε_1 ε_2 in accuracy criterion.

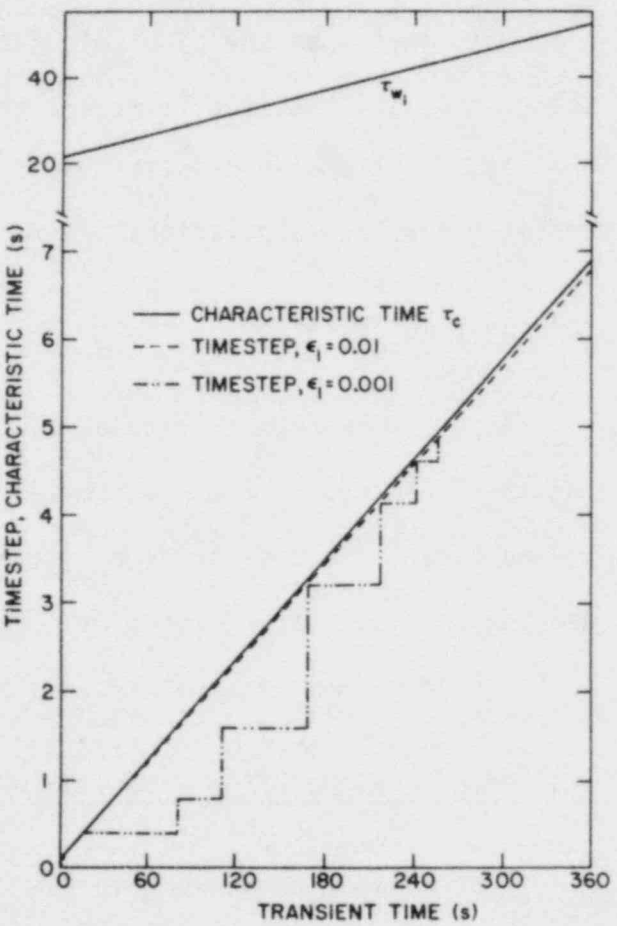

Figure 11. Growth of characteristic time and timesteps for the sample transient

of timestep is governed entirely by τ_c. Since in both cases, the size of timestep remains within the envelope of τ_c, the accuracy of the solution is maintained. The latter calculation, however, required less than one-fifth the computing time used by the former. Hence, it seems advantageous to use τ_c for timestep control.

Also plotted in Fig. 10 is the time constant for T_{w_i}, Eq. (A.8). It is seen to be so large that the explicit formulation of the wall equation, Eq. (7), can be considered stable (and accurate) for all practical purposes.

Note that when the pipe calculations are performed together with the rest of the system, its timestep is restricted by the overall timestep for the heat transport system thermal-hydraulics, which is controlled either by the IHX thermal or system hydraulic calculations.

4.2 System Simulation

A pump coastdown to natural circulation transient in CRBRP was simulated using the SSC-L code. Fig. 12 shows predicted temperatures in the primary system. The combined effect of transport delay, coolant mixing and wall heat capacity in damping the temperature signal is clearly evident from the plots of IHX and reactor vessel inlet temperatures.

4.3 Effects of Modeling Friction in Pipings

Once again, the SSC-L code was used to simulate flow coastdown to natural circulation in CRBRP. An approximate model and a detailed model were used, in turn, to represent frictional losses in the pipings and IHX. Gravity heads and other details were kept the same in both models. In the approximate model, all frictional and form losses (excluding those in reactor vessel) were treated as

$\Delta P = CW|W|$, where C is independent of the flow rate W. In the detailed model, the frictional resistances were explicitly included in the form

$$\Delta P_f = 0.5 \frac{W|W|}{D_e A^2} \int_0^L \frac{f}{\rho} dx, \qquad (33)$$

where f is the friction factor described by Eq. (24) in the turbulent region, and form losses were treated as $\frac{KW|W|}{\rho A^2}$ where K is also a constant. Fig. 13 compares the predicted transient core flow using these models. The scale is considerably expanded to exaggerate small differences. The effect is seen to be small, the results agreeing to within 2%. Note, however, that if friction in the reactor vessel were also included in $CW|W|$, the difference would indeed be very significant, since most of the frictional resistance of the circuit is in the core.

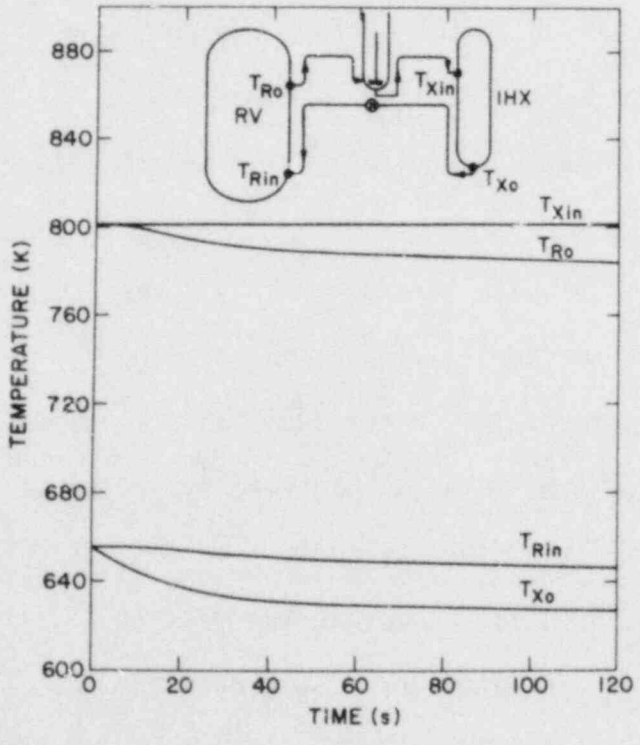

Figure 12. Predicted temperatures in the primary loop for a pump coastdown to natural circulation transient in CRBRP

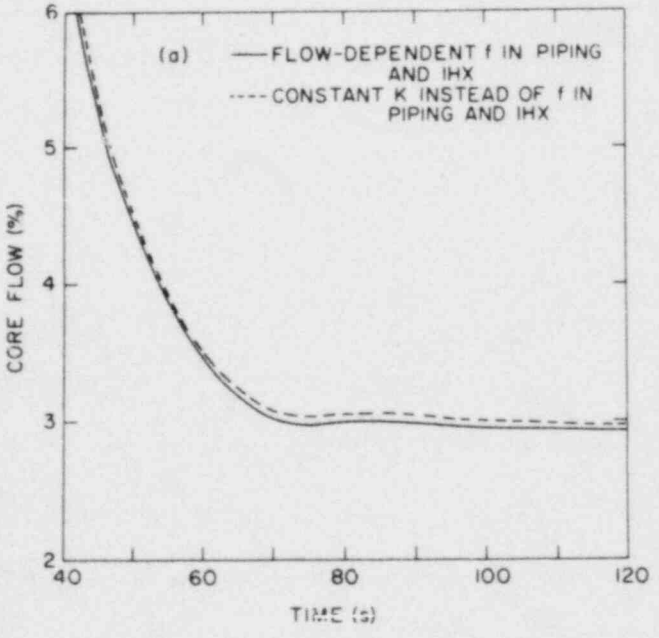

Figure 13. Effect of modeling friction in pipings, IHX on predicted transient core flow.

5. DISCUSSION

A one-dimensional model for coolant flow and heat transfer in the LMFBR sodium-carrying piping has been presented. The model forms an important part of the overall system simulation model. The heat transfer model has several axial nodes and two radial nodes. Energy equations are written for the coolant and pipe wall using the nodal heat balance approach. Perfect insulation is assumed on the wall outer surface. The coolant equation is formulated implicitly, with explicit heat flux, allowing the solution to march in the flow direction without the need to invert matrices. Uncertainties in Nusselt number correlations were seen to have the greatest impact on overall heat transfer coefficients at low flow conditions. Also, in this region, the correlations commonly used exhibit the widest disparity. From the transient cases studied, the following conclusions can be drawn:

1) The coolant, wall model is adequate for system simulation. The added complexity of including insulation losses is not justified; also, the simpler models such as transport-delay and coolant mixing appear to be inadequate.
2) The axial nodalization with the nodal heat balance method is seen to be bounded. A good number to use for system simulation would be $N \geq 2(\theta + 1)$, where θ is the transport time, in seconds, at full flow.
3) Timestep control is found to be most efficiently achieved by restricting the step size to the characteristic time for coolant temperature.
4) The Reynolds number dependence of friction factor in the pipings and IHX is found not to be a sensitive parameter for flow predictions.

For future work, it will be necessary to examine the development of velocity and thermal boundary layers, as well as the heat transfer to the pump casing and

their influence on predictions. Whereas all models used in current system simulation studies are one-dimensional, the impact of multi-dimensional effects such as local stratification and consequent profile distortions should also be evaluated. Recently, Khatib-Rahbar, et al.[26] compared the 1-D heat transfer model presented in this report to a very detailed 3-D calculation[27,28], for a severe thermal transient occurring at the CRBRP evaporator outlet. It was observed for this case that the influence of radial temperature and velocity profile distortions on the axial temperature distribution was small, and the 1-D model was in good agreement with the 3-D predictions. This indicates that the 1-D model may be quite adequate for large system simulation codes. Further work, however, needs to be done to clearly validate this observation.

APPENDIX A

CHARACTERISTIC TIMES FOR COOLANT AND WALL TEMPERATURES

Eq. (1) can be re-written as

$$\rho V C_p \frac{dT_{i+1}}{dt} = WC_p (T_i - T_{i+1}) - U_{cw}A_{cw}\left[\frac{T_i + T_{i+1}}{2} - T_{w_i}\right] \quad (A.1)$$

or

$$\frac{dT_{i+1}}{dt} = \frac{W}{\rho V}(T_i - T_{i+1}) - \frac{U_{cw}A_{cw}}{2\rho VC_p}\left[T_i + T_{i+1} - 2T_{w_i}\right] \quad (A.2)$$

$$= F$$

In Eq. (A.2), the characteristic time for T_{i+1} is obtained as[10]

$$\tau_{i+1} = -\left(\frac{\partial F}{\partial T_{i+1}}\right)^{-1} \quad (A.3)$$

where

$$\frac{\partial F}{\partial T_{i+1}} = \frac{W}{\rho V}\left(\frac{\partial T_i}{\partial T_{i+1}} - 1\right) - \frac{U_{cw}A_{cw}}{2\rho VC_p}\left(\frac{\partial T_i}{\partial T_{i+1}} + 1 - 2\frac{\partial T_{w_i}}{\partial T_{i+1}}\right) \quad (A.4)$$

Assuming upstream temperatures are not influenced by downstream temperatures, we get $\frac{\partial T_i}{\partial T_{i+1}} = 0$.

$$\therefore \quad \frac{\partial F}{\partial T_{i+1}} = -\left(\frac{W}{\rho V} + \frac{U_{cw}A_{cw}}{2\rho VC_p}\right) + \frac{U_{cw}A_{cw}}{\rho VC_p}\frac{\partial T_{w_i}}{\partial T_{i+1}} \quad (A.5)$$

Neglecting $\frac{\partial T_{w_i}}{\partial T_{i+1}}$ simplifies the expression for $\frac{\partial F}{\partial T_{i+1}}$. Note, however, that this term is not always negligible, and could become important in judging the overall system response.

For the present case, neglecting $\frac{\partial T_{w_i}}{\partial T_{i+1}}$ yields

$$\tau_{i+1} = \left(\frac{W}{\rho V} + \frac{U_{cw} A_{cw}}{2 \rho V C_p} \right)^{-1}$$

or

$$\tau_c = \rho V C_p \Big/ \left(W C_p + 0.5 U_{cw} A_{cw} \right) \tag{A.6}$$

The wall energy equation, Eq. (5) can be re-written as

$$\frac{dT_{w_i}}{dt} = \frac{U_{cw} A_{cw}}{M_w C_{w_i}} \left[T_{i,i+1} - T_{w_i} \right] \tag{A.7}$$

The characteristic time for T_{w_i} is obtained as

$$\tau_{w_i} = \left(\frac{U_{cw} A_{cw}}{M_w C_{w_i}} \right)^{-1} \tag{A.8}$$

APPENDIX B

ENERGY BALANCE INCLUDING HEAT LOSSES THROUGH INSULATION

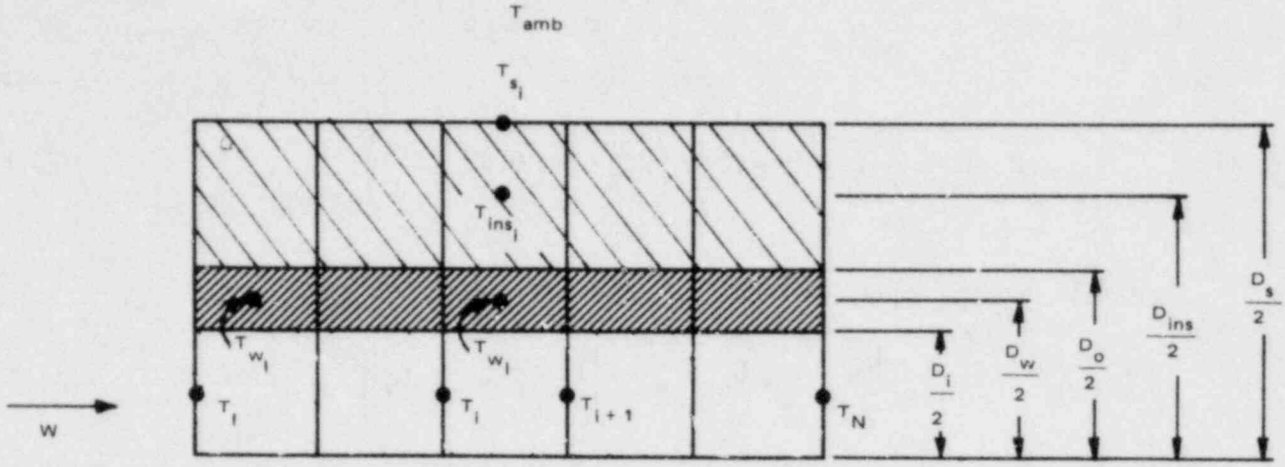

Figure B.1. Model configuration for energy balance with insulation losses.

If heat losses through insulation are included, the wall equation (Eq. (5)) modifies to

$$M_w C_{w_i} \frac{dT_{w_i}}{dt} = U_{cw} A_{cw} \left(T_{i,i+1} - T_{w_i}\right) - U_{wins} A_{wins} \left(T_{w_i} - T_{ins_i}\right) \qquad (B.1)$$

In addition, equations for the insulation and its surface can be written, respectively, as:

$$M_{ins} C_{ins_i} \frac{dT_{ins_i}}{dt} = U_{wins} A_{wins} \left(T_{w_i} - T_{ins_i}\right) - U_{inss} A_{inss} \left(T_{ins_i} - T_{s_i}\right) \qquad (B.2)$$

$$U_{inss} A_{inss} \left(T_{ins_i} - T_{s_i}\right) = (hA)_{sa} \left(T_{s_i} - T_{amb}\right) \qquad (B.3)$$

where the overall heat transfer coefficients are defined by

$$\frac{1}{U_{wins}} = \frac{D_o}{2k_w} \ln \frac{D_o}{D_w} + \frac{D_o}{2k_{ins}} \ln \frac{D_{ins}}{D_o} \tag{B.4}$$

$$\frac{1}{U_{inss}} = \frac{D_s}{2k_{ins}} \ln \frac{D_s}{D_{ins}} \tag{B.5}$$

$$h_{sa} = h_{sc} + h_{sr} \tag{B.6}$$

where h_{sc}, h_{sr} are the convective and radiative components of the surface heat transfer coefficient, as follows[24]:

$$h_{sc} = 0.8512 \, (T_s - T_{amb})^{0.25} \tag{B.7}$$

$$h_{sr} = 2.3035 \times 10^{-9} \, (T_s^4 - T_{amb}^4) \Big/ (T_s - T_{amb}) \tag{B.8}$$

Here, T_s and T_{amb} are in absolute units (K).

Taking advantage of the physical process, we can make the following simplifying assumptions:

a) The insulation and surface temperatures are uniform,

i.e.

$$T_{ins_i} = T_{ins} \, , \quad T_{s_i} = T_s .$$

b) k_{ins}, the insulation conductivity, is constant throughout the transient. Hence, U_{inss} is constant.

Eqs. (1), (B.1) - (B.3) can be solved in a similar manner to the coolant wall equations to obtain the transient response. However, the temperatures at the start of the transient are not as readily obtained as with the coolant, wall

model. Steady state energy balances have to be obtained by setting the time-derivatives of Eqs. (1), (B.1) - (B.3) to zero. Eq. (B.3) can be re-written as

$$T_s = \frac{U_{inss}\, T_{ins} + h_{sa}\, T_{amb}}{U_{inss} + h_{sa}} \tag{B.9}$$

(B.2) reduces to

$$T_{ins} = \frac{D_o\, U_{wins}\, T_{w_1} + D_s\, U_{inss}\, T_s}{D_o\, U_{wins} + D_s\, U_{inss}} \tag{B.10}$$

and Eq. (B.1) reduces to

$$T_{w_i} = \frac{U_{cw} A_{cw}\, T_{i,i+1} + U_{wins} A_{wins} T_{ins}}{U_{cw} A_{cw} + U_{wins} A_{wins}} \tag{B.11}$$

Eq. (1) can be re-written as

$$e_{i+1} = e_i - \frac{U_{cw} A_{cw}}{W} (T_{i,i+1} - T_{w_i}) \tag{B.12}$$

Initial guesses for the temperatures are made, for i = 1 to N - 1, as

$$e_{i+1} = e_1$$

$$T_{i+1} = T_1$$

$$T_{w_i} = T_1 \quad .$$

$$T_s = T_{amb} + 50K$$

$$T_{ins} = (T_{w_1} + T_s)/2$$

T_{amb} is assumed known.

With these guesses, Eqs. (B.9) - (B.12) are solved iteratively, along with equations for U_{cw}, h_{sa}, until convergence given by $|T_s^{new} - T_s^{old}| \leq 0.01K$, is satisfied. This completely specifies the pre-transient conditions.

APPENDIX C

TRANSPORT DELAY CALCULATIONS

The instantaneous velocity of a particle of fluid in the pipe can be written as

$$v = \frac{dx}{dt} \tag{C.1}$$

In addition, if $v = v(t)$ is known, Eq. (C.1) can be integrated as follows:

$$\int_0^L dx = \int_{t_1}^{t_2} v(t)dt \tag{C.2}$$

where t_1 is the time at which the particle or signal originated at the pipe entrance, and t_2 is the time at which it traveled a length L of the pipe.

For the transient analyzed in Chapter 4,

$$v(t) = v_{ref}\left(1 - \frac{t}{t + \delta}\right) \tag{C.3}$$

so that

$$L = \delta v_{ref} \int_{t_1}^{t_2} \frac{dt}{t + \delta} \tag{C.4}$$

or

$$L = \delta v_{ref} \ln\left(\frac{t_2 + \delta}{t_1 + \delta}\right) \tag{C.5}$$

i.e.

$$\frac{t_2 + \delta}{t_1 + \delta} = e^{\frac{L}{\delta v_{ref}}} \tag{C.6}$$

where $$v_{ref} = \frac{W_{ref}}{\rho A}$$

and $$A = \frac{\pi}{4} D_i^2 \qquad (C.7)$$

For W_{ref} = 805.1 kg/s, ρ = 855 kg/m^3, D_i = 0.4318 m, and δ = 5.5, we obtain

$$v_{ref} = 6.43 \text{ m/s, and}$$

$$\frac{t_2 + 5.5}{t_1 + 5.5} = 2.027665 \qquad (C.8)$$

Applying Eq. (C.8) to the input temperature signal of Chaper 4, we generate the values shown in Table C.I below and plotted in Fig. 8 for the outlet signal.

TABLE C.I

Transport Delay Times for the Temperature Signal

Temperature Signal (K)	t_1 (s)	t_2 (s)
616.0	0.0	5.65
552.5	40.0	86.76
520.75	60.0	127.31
489.0	80.0	167.87

REFERENCES

1. C. R. Brinkman, V. K. Sikka, and R. T. King, "Mechanical Properties of LMFBR Primary Piping Materials", Nuclear Technology, 33, No. 1, 78 (1977).

2. "LMFBR Demonstration Plant Simulation Model, DEMO", Westinghouse Advanced Reactors Division, Waltz Mill, Pennsylvania, WARD-D-0005 (Rev. 4), (1976).

3. A. K. Agrawal, et al., "An Advanced Thermohydraulic Simulation Code for Transients in LMFBRs (SSC-L Code)", Brookhaven National Laboratory, BNL-NUREG-50773 (1978).

4. "Clinch River Breeder Reactor Project, Preliminary Safety Analysis Report", Project Management Corporation (1975).

5. L. H. Gerhardstein, "Multi-node Simulation of the FFTF Intermediate Heat Exchanger", Pacific Northwest Laboratory, BNWL-CC-664 (1966).

6. R. F. Clist and A. Hopkinson, in 'Prototype Fast Reactor Primary Circuit and Intermediate Heat Exchanger Dynamic Model', edited by A. Hopkinson, U. K. Atomic Energy Authority, AEEW-R418 (1965).

7. G. J. Jennings. "Mathematical Models of Heat Exchangers", Westinghouse Report FPC-113 (1969).

8. A. L. Gunby, "Intermediate Heat Exchanger Modeling for FFTF Simulation", Pacific Northwest Laboratory, BNWL-1367 (1970).

9. W. J. Karplus, "An Electric Circuit Theory Approach to Finite-Difference Stability", *Trans. AIEE* 77, No. 1 (1958).

10. M. Khatib-Rahbar, "System Modeling for Transient Analysis of Loop-Type Liquid-Metal-Cooled Fast Breeder Reactors", Cornell University, CURL-53 (1978).

11. S. Aoki, "Current Liquid-Metal Heat Transfer Research in Japan", *Progress in Heat and Mass Transfer*, 7, 569-573, edited by O. E. Dwyer, Pergamon Press, Inc., Elmsford, New York (1973).

12. O. E. Dwyer, "Liquid-Metal Heat Transfer", Ch. 2 in *Sodium-NaK Engineering Handbook*, Vol. 2, edited by O. J. Foust, Gordon and Breach, Inc., New York, New York (1976).

13. Kuroyanagi, et al., The 7th Japan Heat Transfer Symposium, 269-272 (1970).

14. R. N. Lyon, *Chem. Eng. Progr.* 47, 75-79 (1951).

15. O. E. Dwyer, "Eddy Transport in Liquid-Metal Heat Transfer", *AIChE Journal*, 9, No. 2, 261-268 (1963).

16. V. I. Subbotin, et al., "A Study of Heat Transfer to Molten Sodium in Tubes", *Atomic Energy*, (USSR) 13, 380-382 (1962).

17. W. M. Kays, *Convective Heat and Mass Transfer*, McGraw-Hill, New York (1966).

18. A. J. Friedland, "Coolant Properties, Heat Transfer, and Fluid Flow of Liquid Metals", Ch. 2 in *Fast Reactor Technology: Plant Design*, edited by J. G. Yevick, The M.I.T. Press, Cambridge, Massachusetts (1966).

19. C. F. Bonilla, "Fluid Flow in Reactor Systems", *Nuclear Engineering Handbook*, pp. 9-30, edited by H. Etherington, McGraw-Hill, New York (1958).

20. H. Schlichting, *Boundary Layer Theory*, 4th edition, p.515, McGraw-Hill, New York (1968).

21. S. Levy, "Fluid Flow", Ch. 15 in *The Technology of Nuclear Reactor Safety*, Vol. 2, edited by T. J. Thompson and J. G. Beckerly, the M.I.T. Press, Cambridge, Massachusetts (1973).

22. W. H. McAdams, *Heat Transmission*, 2nd edition, McGraw-Hill, New York (1942).

23. J. Graham, *Fast Reactor Safety*, Academic Press, New York (1971).

24. H. G. Johnson, "Simulation of Coolant Transport and Heat Exchange in Pipe Runs", Hanford Engineering Development Laboratory, HEDL-TME-75-39 (1975).

25. H. M. Domanus, R. C. Schmitt, and W. T. Sha, "Numerical Results Obtained from the Three Dimensional Transient Single Phase Version of COMMIX Computer Code", Argonne National Laboratory, ANL-CT-78-3 (1977).

26. M. Khatib-Rahbar, I. K. Madni, and A. K. Agrawal, "Impact of Multi-Dimensional Effects in LMFBR Piping Systems", Proceedings of the Specialists Meeting on Decay Heat Removal and Natural Convection in FBR's, Upton, NY, February, 1980, (to be published).

27. D. S. Trent, et al., private communication, Pacific Northwest Laboratory (1979).

28. D. S. Trent, "TEMPEST: A Three Dimensional Time Dependent Computer Program for Hydrothermal Analysis", Informal Report, FATE-79-15, Pacific Northwest Laboratory, Richland, Washington (July 1979).

U.S. GOVERNMENT PRINTING OFFICE: 1980 48